New Expi293 suite of products for structural biology, inducible expression, and protein labeling

Learn more

gibco
by Thermo Fisher Scientific

Comparative NMR study on the impact of point mutations on protein stability of *Pseudomonas mendocina* lipase

NATHALIE SIBILLE,[1,4] ADRIEN FAVIER,[1,4,5] ANA I. AZUAGA,[2] GRANT GANSHAW,[3] RICHARD BOTT,[3] ALEXANDRE M.J.J. BONVIN,[1] ROLF BOELENS,[1] AND NICO A.J. VAN NULAND[2]

[1]Bijvoet Center for Biomolecular Research, Department of NMR Spectroscopy, 3584 CH Utrecht, The Netherlands
[2]Departamento de Química Física, Facultad de Ciencias, Universidad de Granada, 18071 Granada, Spain
[3]Genencor International, Inc., Palo Alto, California 94304, USA

(RECEIVED March 13, 2006; FINAL REVISION April 26, 2006; ACCEPTED April 29, 2006)

Abstract

In this work we compare the dynamics and conformational stability of *Pseudomonas mendocina* lipase enzyme and its F180P/S205G mutant that shows higher activity and stability for use in washing powders. Our NMR analyses indicate virtually identical structures but reveal remarkable differences in local dynamics, with striking correspondence between experimental data (i.e., ^{15}N relaxation and H/D exchange rates) and data from Molecular Dynamics simulations. While overall the cores of both proteins are very rigid on the pico- to nanosecond timescale and are largely protected from H/D exchange, the two point mutations stabilize helices α1, α4, and α5 and locally destabilize the H-bond network of the β-sheet (β7–β9). In particular, it emerges that helix α5, undergoing some fast destabilizing motions (on the pico- to nanosecond timescale) in wild-type lipase, is substantially rigidified by the mutation of Phe180 for a proline at its N terminus. This observation could be explained by the release of some penalizing strain, as proline does not require any ''N-capping'' hydrogen bond acceptor in the i+3 position. The combined experimental and simulated data thus indicate that reduced molecular flexibility of the F180P/S205G mutant lipase underlies its increased stability, and thus reveals a correlation between microscopic dynamics and macroscopic thermodynamic properties. This could contribute to the observed altered enzyme activity, as may be inferred from recent studies linking enzyme kinetics to their local molecular dynamics.

Keywords: NMR; protein stability; protein dynamics; H/D exchange; ^{15}N relaxation; mutation effects

Supplemental material: see www.proteinscience.org

Understanding how each newly synthesized polypeptide chain folds into a unique, active, low-energy protein structure has intrigued scientists for decades (Dobson et al. 1998). There also is considerable industrial interest in this problem: (1) For the production of industrial enzymes, high yields can be obtained only with proper folding; (2) upon storage, these enzymes should maintain their active conformation; and (3) in their application, the proteins have to withstand sometimes harsh industrial conditions—e.g., enzymes in washing powders have to remain active at high temperature in an alkaline environment and in the presence of detergents. Much effort has

[4]These authors contributed equally to this work.
[5]Present address: Institut de Biologie Structurale Jean-Pierre Ebel, Laboratoire de RMN, 38027 Grenoble Cedex 1, France.

Reprint requests to: Nico A.J. van Nuland, Departamento de Química Física e Instituto de Biotecnología, Facultad de Ciencias, Universidad de Granada, Campus Fuentenueva s/n, 18071 Granada, Spain; e-mail: najvan@ugr.es; fax: +34-958-272879.

Abbreviations: CD, circular dichroism; CSI, chemical shift index; DSC, differential scanning calorimetry; HN, amide proton; H/D, proton-deuterium; HSQC, heteronuclear single-quantum coherence spectroscopy; MD, molecular dynamics; NMR, nuclear magnetic resonance; NOESY, nuclear Overhauser enhancement spectroscopy; PG, F180P/S205G mutant lipase.

Article published online ahead of print. Article and publication date are at http://www.proteinscience.org/cgi/doi/10.1110/ps.062213706.

been put into optimizing the ''performance'' of industrial enzymes predominantly by using protein-engineering techniques. Among them are proteases such as subtilisins that degrade proteins, and lipases that hydrolyze a range of complex ester-linked triglycerides. These lipases would be ideal for removing fat-stains in laundry washing (Jaeger et al. 1999). The common challenges for all these industrially relevant enzymes are (1) to obtain stable, active forms and (2) to prevent their inactivation by the conditions at which they have to be active. To address these questions one has to understand the determinants for the structural stability and dynamics, and how the protein of interest folds into an active conformation in a wide range of conditions. Folding studies on proteins such as subtilisins, however, are hampered by their protease activity, resulting in irreversible degradation.

In this study we have focused on lipase from *Pseudomonas mendocina* (Boston et al. 1997), which has originally been classified as a cutinase and is inhibited by diethyl *p*-nitrophenyl, suggesting it is a serine esterase. The gene was cloned and expressed in high quantities from *Bacillus subtilis*. A high-resolution structure of this 27.5-kDa triglyceride hydrolase has been determined by X-ray diffraction (Boston et al. 1997), showing the tertiary fold common to all α/β hydrolases (Fig. 1). A nucleophilic residue (Ser in lipases), conserved His, and an acidic residue Asp or Glu form the active site triad found in this type of enzyme. The β-strands and α-helices are connected by short loops, and the active site that is covered by inserted loops in most lipases remains exposed in *P. mendocina* lipase, as in *Fusarium soloni pisi* cutinase (Prompers et al. 1997) (MW 23 kDa), mimicking the open conformation of other lipases. *P. mendocina* lipase therefore was selected for protein engineering to produce an improved enzyme for use in detergents. X-ray diffraction studies of several mutants show no significant

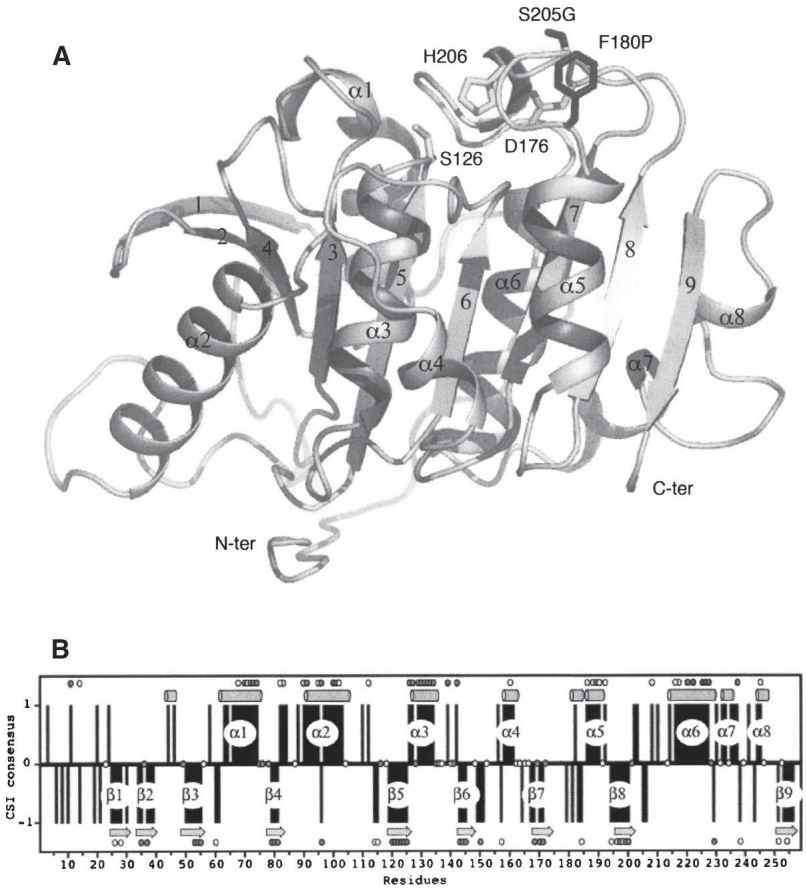

Figure 1. Structure of *P. mendocina* lipase. *(A)* X-ray structure of the wild-type protein (PDB entry 2FX5). (Light gray sticks) The catalytic triad formed by Ser126, His206, and Asp176; (dark gray sticks) the two mutations in PG. *(B)* Secondary structure of the wild-type lipase deduced from Chemical Shift Index (CSI) analysis compared with the secondary structure elements present in the X-ray structure. The CSI consensus is represented by the black histogram along the wild-type lipase sequence. The helix and strand cartoons correspond to the X-ray secondary structure of the enzyme. The light and dark gray dots highlight wild-type residue backbone NH protected from the solvent from hours to weeks and for >2 mo, respectively.

structural differences; modification of the substrate-binding surface most likely increases binding of the extra acyl side chain of triglyceride substrates (Boston et al. 1997). The cleaning power degrades in the presence of anionic surfactants such as linear alkyl benzene sulfonates (LAS). The F180P/S205G mutant (PG mutant), however, shows a higher activity and stability in the presence of washing powders.

The goal of the current study is to understand the underlying features of the stability and activity increase engendered by point mutations using comparative NMR studies, yielding information in solution state with atomic resolution. In the work described here, we performed H/D exchange and ^{15}N relaxation experiments to characterize the stability and mobility of a wild-type lipase and an engineered double mutant, and complemented the experimental findings by other biophysical techniques and long MD simulations in explicit solvent.

To summarize the main results, we demonstrate that the lipase has a high tendency to aggregate, especially at elevated temperatures, and most probably has protease activity, which results in self-degradation. These two factors are likely the cause of the low cleaning power of these enzymes. The higher enzymatic activity and stability against detergents of the PG mutant can, at least partially, be explained by the lower tendency of this protein to aggregate, which likely results from the increase in thermodynamic stability engendered by altered local dynamics, entailed by the two point mutations. The higher stability and the aggregation phenomena of this protein were confirmed by other biophysical techniques (CD, DSC, and fluorescence). More specifically, these data indicate that the double mutation stabilizes helices α1, α4, and α5, confirmed by the relaxation data and MD simulations; the stabilization of the fifth helix can be rationalized by the favored N-capping of the proline residue.

Results

Both wild-type and a F180P/S205G double mutant (PG) lipase with higher activity and stability were studied. NMR experiments were carried out at 313 K on a 600 MHz spectrometer equipped with a cryo probe, unless stated otherwise.

Sample stability

In the 2D ^{15}N-HSQC spectra of 258-residue *P. mendocina* wild-type and PG mutant lipase, the large dispersion in both ^{15}N and ^{1}H dimensions indicates a high degree of β-strand structure. The spectra of both proteins are very similar, suggesting corresponding 3D structures. Both samples, however, proved unstable over a 3-d period, preventing NMR assignment using standard protocols. ^{15}N-HSQC spectra of a freshly prepared sample stored for 3 d at 313 K show the appearance of signals near random coil frequencies. SDS gels of fresh samples produced the expected single band corresponding to monomeric lipase, whereas several bands of lower molecular weight appeared after 3 d, most probably attributable to cleaved protein fragments. Adding the specific inhibitor diethyl p-nitrophenyl phosphate (commercial name *E600*), however, stabilized the protein samples for up to several months. It may be envisaged that both wild-type and PG mutant lipase could experience autocatalytic degradation and not degradation caused by an external protease contaminant since addition of the specific and irreversible inhibitor *E600*, but not of standard protease inhibitors, prevents degradation. All further NMR studies were therefore carried out in the presence of *E600*. The ^{15}N-HSQC of free and *E600*-bound wild-type lipase reveal a large number of shifting peaks, of which the most strongly shifting ones mainly correspond to residues near the active site (data not shown). Interestingly, changes in the ^{15}N-HSQC from covalent inhibitor binding occur only after 4–5 h when adding *E600* to equimolar quantities, indicating a rather high activation barrier. It could be due to the requirement of substantial conformational rearrangements within the binding site of lipase, which would be in line with the observed abundance of induced chemical shift changes.

We furthermore noticed that lipase had a strong tendency to aggregate under the initially chosen conditions. The low solubility of the protein limited the sample concentration in our studies to less than ~0.7 mM. Small variations in salt concentration toward low concentration dramatically improved the quality of the NMR spectra. At higher acetate concentration line widths broaden, apparently due to reversible protein association. At low acetate concentration the NMR lines sharpen, and the ^{15}N-HSQC spectrum then corresponds to the monomeric form of the protein, as later verified by relaxation measurements.

Backbone assignment of wild-type and PG mutant lipase

All 3D triple resonance NMR experiments for backbone assignment were recorded on a 600-MHz spectrometer equipped with a cryo probe, where the higher sensitivity was essential to accumulate enough signal intensity. The lipase PG mutant backbone was assigned first since its NMR spectra were of higher quality in general. A first set of 3D experiments was recorded at 303 K, allowing the assignment of nearly all residues except for those located around the active site. These missing signals, however, showed up in spectra recorded at 313 K, indicating line broadening from slow conformational mobility as likely cause for their disappearance at 303 K. It was then possible to assign all HN, N, CA, and CB chemical shifts (for

non-proline residues) except for the N-terminal Ala1, which is followed by a proline. In addition, backbone CO frequencies could be assigned for all residues except those followed by a proline. The backbone assignment of the wild-type lipase was then straightforward, assisted by the chemical shift assignments of the spectrally very similar PG mutant (data not shown), and as complete as for the PG mutant, except for Phe180, which was either too weak to be detected or overlapped with another spin system.

The Chemical Shift Index (CSI) analysis of the PG lipase CA, CB, and CO frequencies (Wishart and Sykes 1994) shows that its secondary structure in solution and in the crystal are closely similar (Fig. 1B). However, helices α2 and α6 and the β-strands β6 and β7 seem slightly shorter in solution. Additionally, the short helical region comprising residues 181–184 in the X-ray structure is not confirmed by CSI analysis. The CSI analysis of the wild-type lipase CA, CB, and CO frequencies yielded analogous results.

Backbone dynamics from ^{15}N relaxation data

^{15}N NMR relaxation data are sensitive probes for both molecular rotational diffusion and local backbone dynamics of a protein. We measured ^{15}N R_1 and R_2 relaxation rates as well as the $^{15}N\{^1H\}$ NOE at 600 MHz and 313 K, and evaluated the data qualitatively by reduced spectral density mapping (Peng and Wagner 1992; Farrow et al. 1995; Ishima et al. 1995). The anisotropy of the rotational diffusion was analyzed with TENSOR2 (Dosset et al. 2000), using exclusively data from rigid residues within elements of secondary structure that did not display any significant chemical shift changes in the ^{15}N-HSQC upon *E600* binding or due to the PG mutations.

First visual inspection of the ^{15}N-HSQC spectra of 0.6 mM wild-type and PG lipase already revealed substantial line-broadening for wild type, indicating its increased tendency to aggregate. This was corroborated by the analysis of relaxation data recorded for both proteins at 0.6 mM concentration, where average ^{15}N R_2/R_1 ratios yielded apparent rotational correlation times τ_m of 19.00 ± 0.05 nsec for wild type, almost twice as long as the 10.57 ± 0.05 nsec obtained for PG. At 0.2 mM, R_2 rates of wild type become comparable to PG at 0.6 mM. The extracted τ_m of 9.37 ± 0.05 nsec is then within the expected range for a monomeric 28-kDa protein, while ~13% shorter than the τ_m determined for PG at 0.6 mM. This likely indicates minor aggregation for PG that is, however, much less severe than for wild type at the same 0.6 mM concentration but might still demand some caution when interpreting the pertaining relaxation data (Korzhnev et al. 2003). Other than a general offset in relaxation rates that could easily be corrected, aggregation mostly affects the anisotropy of the molecular diffusion tensor and may thus bias the structure-based back-calculation for relaxation rates. As the molecular correlation time of PG lipase was comparable at 0.2 and 0.6 mM concentration, we continued our relaxation measurements on the 0.6 mM sample for reasons of sensitivity; wild-type lipase in contrast required the lower 0.2 mM concentration for ensuring a stable minimal correlation time. Axially symmetric molecular tumbling best fitted the relaxation data of the selected residues assumed to be rigid. The diffusion tensors derived for PG and wild type (Table 1) agree within their statistical errors, corroborating structural congruence between both proteins. Still, the extent of anisotropy $D_{//}/D_{\perp}$ appears slightly increased for PG, in line with a possible, yet obviously very small, bias from minor aggregation (see above).

With the aim of compactly visualizing differences in local dynamics between wild-type and PG lipase, we analyzed the ^{15}N relaxation data by means of reduced spectral density mapping at J(0), $J(\omega_N)$, and $J(\omega_H+\omega_N)$ values (Peng and Wagner 1992; Farrow et al. 1995; Ishima et al. 1995). Both the low-frequency $J(\omega_N)$ versus J(0) and the high-frequency $J(\omega_H+\omega_N)$ versus J(0) spectral density maps are shown in Figure 2. For PG and wild-type lipase, respectively, 178 (69%) and 139 (54%) of the 258 residues in total were analyzed. For PG (Fig. 2A), three different classes of residues with similar dynamics may be identified from inspection of both spectral density maps in combination. The largest group I contains 153 residues (86% of all sampled residues) without notable local dynamics; these residues lie mostly within the structured core of the protein comprising the β-sheet and all eight α-helices. The four residues in group II (2.2%) are mostly located in loops and have large J(0) values (corresponding to a shift to the right in both spectral density maps) indicative of conformational exchange contributions. Group III comprises 21 residues (11.8%) with motions on a fast (picosecond to nanosecond) timescale that reduce J(0) (resulting in a shift to the left in both spectral density maps). Figure 2 (bottom) shows the projection of the residues within both mobile groups II and III onto the X-ray structure of wild-type lipase (using the same color code). For wild-type lipase (Fig. 2B), we identified five (3.6%) and eight (5.8%) residues in

Table 1. *Anisotropic diffusion tensors obtained for wild-type and mutant lipase from the NMR relaxation data analysis using TENSOR2*

	PG (0.6 mM)	Wild type (0.2 mM)
Phi (°)	−88 ± 3	−83 ± 6
Theta (°)	−40 ± 3	−37 ± 3
$D_{\perp}$ (MHz)	14.1 ± 0.7	16.4 ± 1.0
$D_{//}$ (MHz)	19.5 ± 1.0	21.0 ± 1.3
$D_{//}/D_{\perp}$	1.39 ± 0.10	1.28 ± 0.11

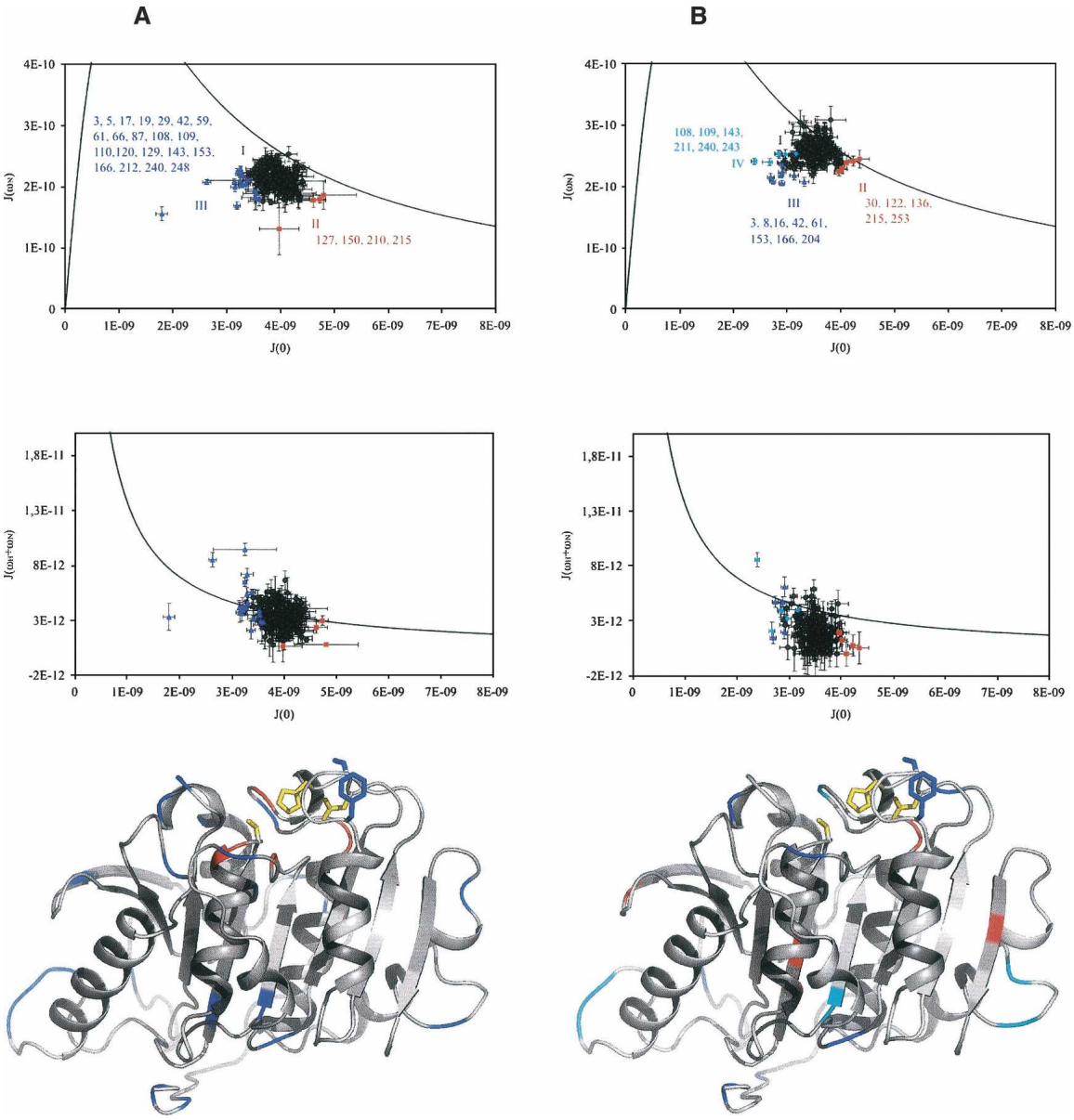

Figure 2. Reduced spectral density mapping. Plot of $J(\omega_N)$ (*top*) and $J(\omega_H+\omega_N)$ (*middle*) versus J(0) for PG (*A*) and wild type (*B*). Results are mapped onto the X-ray structure (*bottom*; same color code). Outlier residues experiencing fast (picosecond to nanosecond) and slow (microsecond to millisecond) local motions are indicated. The residues of group I are colored in gray; all residues of other groups are colored in red for group II, in blue for group III, in white if no data are available, and in the case of wild type, in cyan for group IV. The group numbers in brackets, together with the observed type of internal motions, are indicated. (Yellow sticks) Catalytic triad formed by Ser126, His206, and Asp176; (blue sticks) the two mutations in PG.

groups II and III, respectively, plus one additional group IV (six residues = 4.3%) displaying sub-nanosecond motions.

Comparing the structural distribution of mobile residues for PG and wild-type lipase (Fig. 2), we observe an overall high level of rigidity for the protein core, and a congruent clustering of fast local motions mostly in loop regions. Contrarily, slow motions appear to cluster more compactly near the catalytic site for PG (i.e., Gln127 at the N terminus of helix α3, and Tyr150, Val210, and Ala215 within loops), while some isolated residues within the β-sheet are also affected for wild-type lipase. There, both Thr122 (in the center of strand β5) and the juxtaposed Gly136 (near the C terminus of helix α3), as well as Glu30 (at the C terminus of strand β1) and Val253 (in the center of strand β9) display elevated J(0) values indicative of slow conformational mobility.

Interestingly, Ser29 (strand β1) and Val120 (strand β5) in PG lipase display some fast mobility; these residues lie next to Glu30 and Thr122 that, contrarily, show slow conformational mobility in wild-type lipase.

Differences in local dynamics between wild-type and PG lipase may also be revealed in a direct and concise way by comparing R_2/R_1 ratios, which reflect the apparent local correlation time (Kay et al. 1989). A local increase in the R_2/R_1 ratio is indicative of slow conformational motions on the microsecond to millisecond timescale, causing an increase in R_2. Contrarily, a decrease in R_2/R_1 reveals fast local motions with correlation times of 10^{-2} to 10^2 nsec. The sequential plot of the ratios of $(R_2/R_1)_{(PG)}/(R_2/R_1)_{(WT)}$ is shown in Figure 5A (below), revealing those residues for which mobility is significantly different in both proteins. While the differently mobile residues already identified by comparison of spectral density mapping (Fig. 2) show the expected deviation (e.g., Asp5, Gln127, Gly136, and Val210), a few more residues with significantly altered mobility emerge additionally: Leu68 (in the center of helix α1), Gly129 (near the N terminus of helix α3), Leu183 (near the N terminus of helix α5), and Arg201 (C terminus of β8). The changes in the R_2/R_1 ratio for Leu183 (α5), Gly129 (α3), and Leu68 (α1) are exclusively caused by local mobility in wild-type lipase. There, a significantly increased R_1 rate for Leu183 (α5), and R_2 rate for Gly129 (α3) and Leu68 (α1), indicate reduced rigidity relative to PG lipase on fast (picosecond to nanosecond) and slow (microsecond to millisecond) timescales, respectively.

Hydrogen/deuterium exchange measurements and protein stability

Hydrogen/deuterium (H/D) exchange measurements are widely used to assess the stability of a protein and monitor processes such as folding and binding, where the measured exchange rates can be directly converted into stability parameters for individual residues (Bai et al. 1995b; Bai and Englander 1996; Chamberlain et al. 1996). We accordingly studied H/D exchange for both wild-type and PG lipase in their *E600*-bound forms, and derived local protection factors and Gibbs energies (ΔG) values for amenable residues exchanging on an intermediate timescale of hours to several days. For wild-type lipase, 82 of the 238 assigned backbone amide protons did not exchange with the solvent even after 2 mo, while 102 amide protons exchanged quickly within 10 min after dissolving the lyophilized protein in D_2O. Quantitative H/D exchange rates could therefore be determined for 54 residues only. Apart from both peripheral strands β1 and β9 delimiting the β-sheet, the protein core is largely protected from the solvent, with 53 residues showing exchange too slow to be analyzed in terms of quantitative exchange rates. Within the β-sheet, among residues that appear to lie at the ends of the β-strands, only residues Cys34 and Glu200 exchanged too rapidly, while residues Val196 and Trp198 connecting β8 to the C-terminal strand β9 and Val 194 slowly exchange with the solvent within 4 d to 1 mo. Amide protons within the four longer α-helices α1 (68–74), α2 (93–105), α3 (127–135), and α6 (220–229) were also found to exchange only very slowly, i.e., after 4 d. While the H-bond network stabilizing secondary structure in the core of lipase was found to be rather inert to H/D exchange, the loops and short helices, such as α4, α7, and α8 and the N terminus of helix α2 (63–67), generally exchanged too rapidly for extracting protection factors. Nonetheless, some slowly exchanging amide protons could be identified within loops (comprising residues 47–49 and 75–78) that are buried within the lipase structure, but also within loops exposed to the solvent (comprising residues 104–106, 135–141, and 162–166), the two latter loops being located next to each other in the structure.

For PG mutant lipase, H/D exchange characteristics were found to be quite similar to wild type for most residues. In particular, fast (i.e., <10 min) and very slow (i.e., >2 mo) exchanging residues are identical except for six residues whose H/D exchange rate could not be extracted from the NMR experiments for both enzymes: The amide proton of residues Ser158 (N terminus of helix α4) completely exchanged within 10 min in wild-type lipase, but was fully protected against exchange in the PG mutant. Contrarily, residues Ser172 (in strand β7), Glu200 (β8), and Glu254 (β9) in wild-type lipase were still protected against exchange even after 2 mo, while rapidly exchanging within 10 min in the PG mutant. Finally, Val204 exchanged slower than 60 d in PG but has an exchange rate of 30 d in wild type, whereas Glu208 was still protected after 1 mo in wild type, while fully exchanged after a few minutes in PG. Figure 3 summarizes the differences in H/D exchange between both proteins as differences in free energies that can be derived from the corresponding protection factors (data not shown; see Materials and Methods). This projection onto the wild-type structure reveals that mostly the two parallel, adjacent short helices α4 and α5 are more stabilized in the PG mutant, as are residues Asn56 (near the C terminus of β3) and Tyr216 (near the N terminus of helix α6) located in the vicinity of the catalytic triad. Contrarily, the three residues with faster H/D exchange in the PG mutant are located in the same region of the β-sheet (i.e., within strands β7–β9). To a smaller extent, terminal parts of helices α2 and α8 likewise appear more stabilized in wild-type lipase.

Urea- and heat-denaturation measurement and protein stability

To confirm the higher stability of the PG mutant measured by NMR, we performed both urea- and heat-denaturation experiments monitored by fluorescence

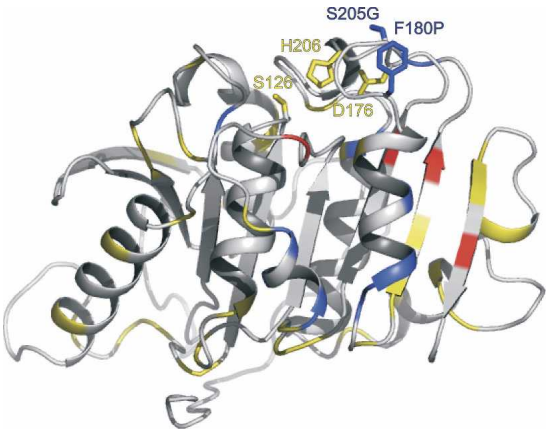

Figure 3. Difference in protection against H/D exchange between the wild-type and PG mutant lipase. Differences are depicted as differences between the free energy differences ($\Delta\Delta G = \Delta G_{PG} - \Delta G_{WT}$) of PG mutant and wild-type lipase projected on the wild-type X-ray structure. Residues with $\Delta\Delta G > 1$ kcal/mol (red), with $\Delta\Delta G < -1$ kcal/mol (blue), and with $-1 < \Delta\Delta G < 1$ kcal/mol (yellow). (Yellow sticks) Catalytic triad formed by Ser126, His206, and Asp176; (blue sticks) the two mutations in PG.

and far-UV CD. The unfolding induced by urea was found to be fully reversible. However, the fluorescence increase at low urea concentrations up to ~2 M urea indicates a transition from the native state toward an intermediate state, which then unfolds into the denatured state at higher urea concentrations (Fig. 4A). If one discards the pre-transition, the unfolding transition can be analyzed using a two-state model (Fig. 4B). Such analysis has been performed in studies of other proteins, e.g., for HPr (Van Nuland et al. 1998). An approximate value for the free energy of unfolding can be obtained from such an analysis of the wild-type protein in the presence of *E600* corresponding to 47 ± 10 kJ/mol, which is in the same order as the highest values obtained from the NMR H/D exchange experiments, which are ~40 kJ/mol. Such an analysis was also performed for the wild-type protein in the absence of the inhibitor, resulting in a decrease in the concentration of urea at the midpoint of the transition, *Cm*, of 0.3 M (data not shown). The *Cm* of the PG mutant in the presence of *E600* was found to be ~0.2 M higher than that of the wild-type protein in the presence of *E600* (data not shown), in agreement with the increase in stability upon mutation.

In contrast to the urea denaturation, heat denaturation was found to be irreversible (Fig. 4D). At temperatures above the transition midpoints, irreversible aggregation occurred, which prevented a full thermodynamic analysis of the transition curves. However, a rough estimation of the melting temperatures can be obtained from melting curves such as those in Figure 4D. The melting temperature (T_m) of the PG mutant is estimated to be ~57°C, 4°C higher than that of the wild-type protein. The same increase in T_m was found in DSC experiments (data not shown). Irreversibility due to aggregation was also observed in these DSC experiments as well as in fluorescence experiments and for the proteins in the absence of *E600* (data not shown).

Molecular dynamics simulation and protein stability

In order to get more insight into the structural and dynamical differences between wild-type and the double mutant lipase, 20-nsec MD simulations were performed in explicit solvent (water) (see Material and Methods for details). Both systems are stable within the timescale of the simulation. Non-bonded energies and RMSDs from the starting crystal structure (see Supplemental Fig. S1) indicate that a plateau is reached after ~10 nsec. All further analysis was therefore performed on the 10- to 20-nsec segment. The average backbone RMSDs from the crystal structure over the last 10 nsec are 1.75 ± 0.10 Å and 1.85 ± 0.10 Å for wild type and PG, respectively, and their non-bonded energies are comparable. An analysis of the secondary structure content as a function of time also reveals the stability of the two proteins (Fig. 5B). However, some small but significant differences are revealed: The proline mutation at position 180 results in a clear stabilization of helix α5 (181–191), which can be explained by better helix capping properties. Helix α1 (62–75) also appears to be stabilized in the PG mutant. This stabilization is reflected in the differences in B-factor between wild type and PG (see Supplemental Fig. S2C): A decrease in fluctuations in the PG mutant is observed in the loop preceding helix α1 (60–65), which also affects the interacting loop (86–89) preceding helix α2. The origin of this stabilization, however, remains unknown. Other subtle differences are observed in the stability of helices α4 (157–166) and of β-strands 7–9 (residues Ser172, Glu200, and Glu254). These observations are consistent with the H/D exchange results. We also compared differences in Cα atom fluctuations (see Supplemental Fig. S2) between the two runs: Besides differences in the C and N termini, three regions of the PG mutants corresponding to the loops around the active site (150–160, 175–185, and 200–220) are showing increased flexibility. This increased flexibility, which might affect the active site accessibility, could be associated with the increased activity of the PG mutant.

Discussion

The *P. mendocina* lipase studied here hydrolyzes ester bonds in a broad variety of compounds with an exceptionally accessible catalytic triad (Ser126, His206, and Asp176) located at the surface of the protein (Fig. 1).

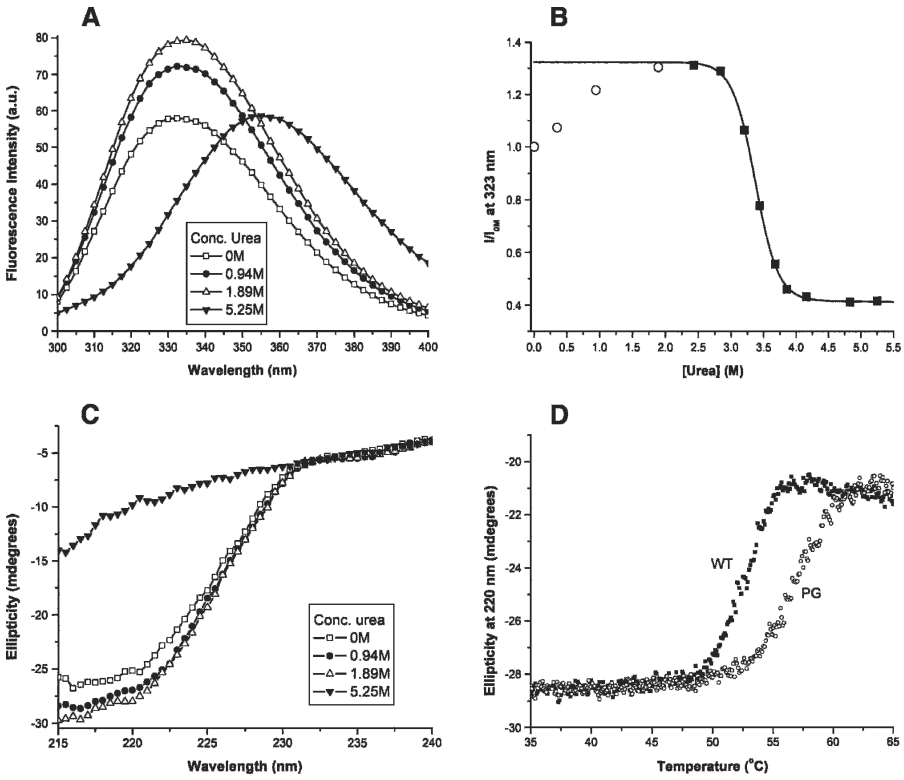

Figure 4. Urea and heat denaturation of wild-type and PG mutant lipase. (*A*) Fluorescence spectra of wild-type lipase in the presence of *E600* at indicated urea concentrations. (*B*) Urea denaturation of wild type: *E600* monitored by fluorescence at 323 nm (*I*) normalized to the intensity at 0 M urea (I_{0M}). The solid line represents the best fit to the data points (filled squares). Points at low urea concentrations (<2 M) were omitted from this analysis (open circles). (*C*) Far-UV CD spectra of wild-type lipase in the presence of *E600* at indicated urea concentrations. (*D*) Heat denaturation measured by CD at 220 nm for wild-type lipase (filled squares) and the PG mutant (open circles). Note that at high temperatures the ellipticity increases due to aggregation of the protein, preventing a complete thermodynamic analysis of the transition curves. These aggregation phenomena were also observed in DSC measurements.

Mutations were introduced to enhance its stability and activity as a potential agent in washing powders; the F180P/S205G (PG) double mutant was found with substantially more favorable characteristics than wild type. Here, Phe180 at the N terminus of helix α5, near the catalytic site, was substituted for a proline that cannot act as H-bond donor, and thus favors distinct ϕ/ψ angles. The polar Ser205, direct neighbor of His206 that is part of the catalytic triad, was replaced by a glycine that can adopt virtually any ϕ/ψ angles. The object of this study was to gain insight into the nature of the stabilization and enhanced activity of the PG mutant lipase using solution-state NMR and complementary biophysical techniques.

At first we noted apparent auto-degradation within a few days of both wild-type and PG lipase that could be prevented by adding the specific inhibitor *E600*. This auto-degradation could not be prevented, however, using the commercially available standard protease inhibitor kits. *E600* binds covalently to lipase, apparently with a high activation energy (causing a slow onset of entailed NMR spectral changes), and causes relatively widespread changes in the ^{15}N-HSQC. The CSI analysis, however, showed that besides some apparent differences in the length of a few secondary structural elements, the *E600*-bound lipase structure in solution is closely similar to the known X-ray apo-structure of wild-type lipase. Spectral differences between *E600*-bound wild-type and PG lipase were quite small and, moreover, no differences in the CSI could be detected, suggesting that the PG double mutation has only small effects on the lipase structure. This conclusion is supported by the nearly identical anisotropic diffusion tensors obtained for both proteins from the NMR relaxation data analysis using TENSOR2, and by the results of the MD simulations.

A difference in physical properties between wild-type and PG lipase was first noted in the ^{15}N-HSQC spectra that revealed substantially enhanced aggregation for wild type at 0.6 mM concentration, requiring us to repeat measurements at 0.2 mM. The PG double mutation thus clearly stabilizes the monomeric form, as later also shown by ^{15}N relaxation studies and complementary CD, fluorescence, and DSC measurements. These biophysical

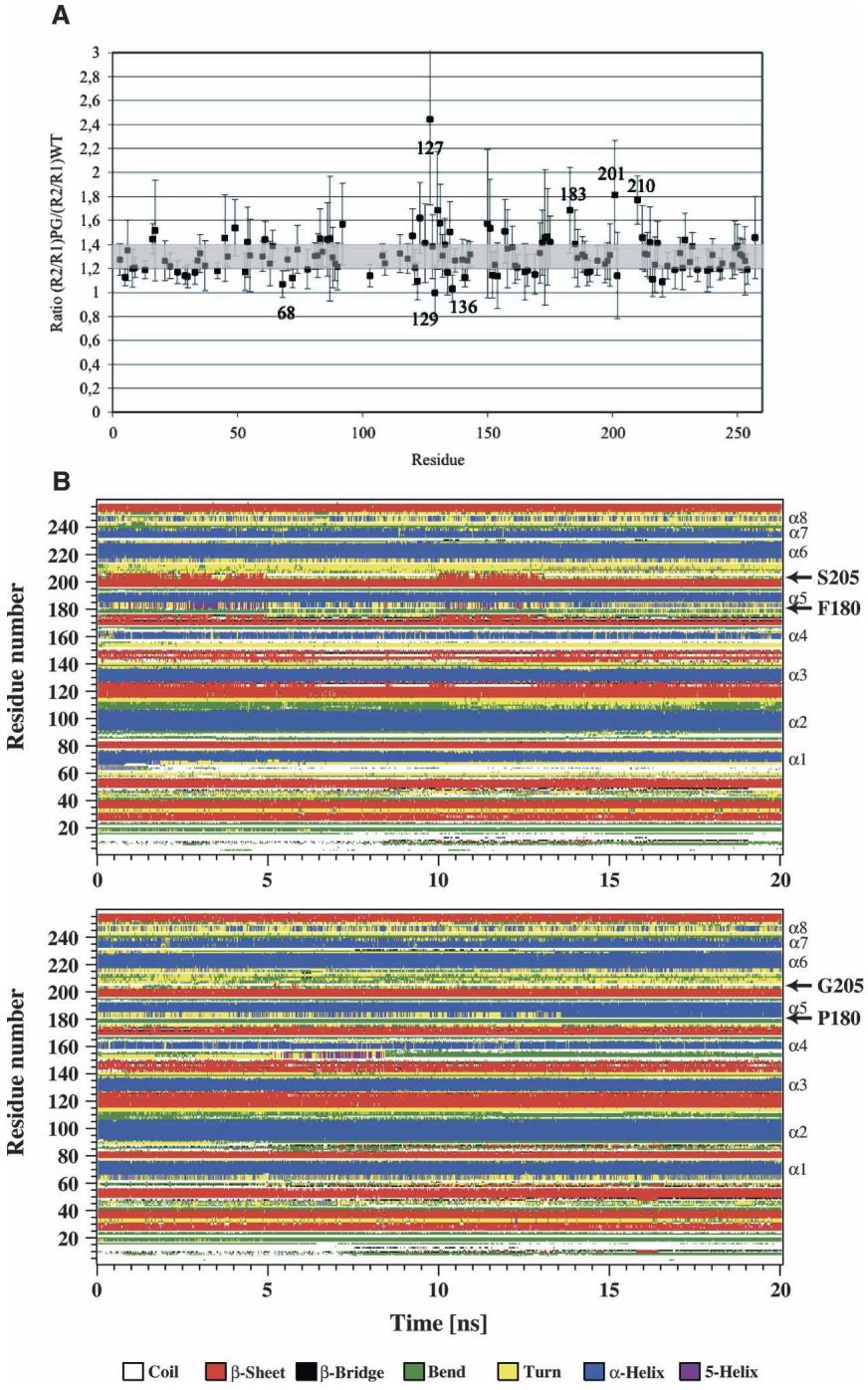

Figure 5. Comparison of molecular dynamics simulations and experimental NMR relaxation data for lipase PG and wild-type. *(A)* $(R_2/R_1)_{(PG)}/(R_2/R_1)_{(WT)}$ ratios. Gray box frames the region of the corresponding average value ± standard deviation. *(B)* Stability of secondary structure elements as a function of time during MD simulations for wild-type (*top* panel) and PG mutant (*bottom* panel) lipase.

techniques were used to obtain a more detailed thermodynamic description of the lipase stability (Fig. 4). It was found that PG lipase unfolds at a substantially higher temperature than wild-type lipase (Fig. 4D). We faced, however, two complications in using these techniques to monitor the unfolding by either chemical denaturant (urea) or heat. First, irreversible aggregation in temperature-induced unfolding experiments prevented the

complete thermodynamics analysis at temperatures above the transition midpoints. This aggregation seems to occur from the unfolded state of lipase, as indicated by the increase in ellipticity at high temperature (Fig. 4D). The observed higher stability of the PG mutant against heat denaturation might therefore at least partially explain its lower tendency to aggregate. Second, even though the unfolding by urea was found to be fully reversible, fluorescence data clearly showed the accumulation of an intermediate state at moderate urea concentrations (Fig. 4). The spectrum of the intermediate state is slightly red-shifted compared with the native state, reflecting a higher water exposure of one or more tryptophans. It also shows a higher fluorescence quantum yield that likely reflects the difference in quenching processes experienced by the tryptophan(s) in the different states. The increased intensity observed in the fluorescence experiments is accompanied by a gradual increase in ellipticity at 220 nm in the far-UV CD spectra of the lipase from 0 to 2 M urea (Fig. 4C), indicating a slight increase of helical structure in the intermediate state. To get a more detailed picture, we recorded ^{1}H-^{15}N-HSQC spectra of lipase in the absence and presence (1 and 2 M) of urea. Most signals are not affected by the addition of urea (data not shown), but amide proton signals from several residues in the N-terminal part of the protein, especially those of residues 16, 17, 20, and 21, shift substantially. The downfield shift of their H^N frequency indicates involvement in hydrogen bonding, which is in line with the change toward an α-helical structure. At least one (unassigned) tryptophan side chain signal shifts substantially upon addition of urea (data not shown), in line with the changes in fluorescence observed at low urea concentrations. The exact structure of this intermediate state would require a more thorough examination, but from the results obtained so far we can conclude that the initial step in the unfolding of lipase by urea involves a local opening of the structure, which increases the accessibility of at least one of the tryptophan side chains to the solvent, with a concurrent formation of a possible α-helical structure in parts of the N terminus. Such a near-native intermediate was also found in the folding of a much smaller globular protein, HPr (Van Nuland et al. 1998; Azuaga et al. 2003). Although differences between the intermediate and the native state may be very small, locally non-native folded regions could well contribute to properties of the protein such as sensitivity to proteolytic cleavage or tendency to aggregate, as observed here.

We next performed ^{15}N relaxation studies to monitor fast motions on the picosecond to nanosecond and microsecond to millisecond timescales, and monitored H/D exchange to assess the conformational stability on a much slower timescale. For both wild-type and PG lipase, the protein core comprising the nine-stranded β-sheet and the longer, central four long helices α1–α3 and α6 appears very rigid from our ^{15}N relaxation studies, and from high protection against H/D exchange. Yet, a few residues in the β-sheet (Glu30 in β1, Thr122 in β5, and Val253 in β9) display slow conformational mobility in wild-type lipase only (Fig. 2B); their neighbors Ser29 and Val120 show mobility on a faster timescale. Thus, the lipase core appears to be somewhat rigidified in the PG double mutant. In contrast, the substrate binding region around the catalytic site appears to be conformationally more flexible on the slow (microsecond to millisecond) timescale in PG lipase (Fig. 2A), putatively making it more amenable to induced-fit adjustment upon substrate binding (Prompers et al. 1999), which in turn could account for the higher activity observed for the double mutant.

A very remarkable dynamics feature emerging from comparative analysis of the ^{15}N relaxation and H/D exchange data is the apparent rigidification and stabilization of the N-terminal part of helix α5 in the PG mutant lipase, where Leu183 lacks the mobility on the fast picosecond to nanosecond timescale found in wild-type lipase, and H/D exchange of Gln186 is almost a magnitude slower. These findings agree strikingly well with our MD simulations that indicate a stabilization of this helix region after F180P mutation on exactly the same nanosecond timescale (Fig. 5). Arguably, the replacement of a (bulky) phenylalanine for a proline without H^N donor capacity at the very N terminus of the helix contributes to its stabilization by relieving some penalizing N-capping requirements (Aurora and Rose 1998). Increased stability in the PG mutant is furthermore indicated within helices α1 and α3 by a lack of slow conformational mobility for Leu68, and Gly129 and Gly136 (Fig. 5A), and within helix α4 by significantly slower water exchange for Ser158, Ser160, and Arg162, and within helix α6 (Tyr216) (Fig. 3). Again, our MD simulations corroborate this experimentally observed stabilization of helices α1 and α4. In contrast, Figure 3 reveals some local destabilization of the β-sheet (strands β7-β9) and helix α8 in PG lipase. Remarkably, the affected residues are close neighbors in space, such that their enhanced susceptibility to H/D exchange might be correlated. Furthermore, this cluster of residues is close to the stabilized residues in helices α4, α5, and α6, suggesting a reciprocal correlation. The latter stabilization in PG lipase would thus come at the expense of some destabilization in the peripheral β-sheet.

In summary, we have shown that the two F180P/S205G point mutations significantly enhance the stability of *P. mendocina* lipase. The enhanced stability under denaturating conditions (e.g., heat or increased urea concentration) strongly reduces the tendency of PG lipase to aggregate, which appears to primarily occur from the unfolded state. Our NMR analyses show that the mutation

entails virtually no changes in the lipase structure; rather, these two point mutations effect distinct local changes in protein flexibility. Both experimental and simulated data indicate that, in PG lipase, helices α1 (residues 62–75), α4 (residues 157–166), and α5 (residues 181–185) are stabilized, while the H-bond network of the β-sheet might be somewhat destabilized locally (i.e., in strands β7–9). In particular, the observed stabilization of helix α5 in the PG lipase could be well understood by the assumption that the substitution of Phe180, at the beginning of α5, for a proline significantly relieves penalizing strain by alleviating the need for N-capping. Overall, the correspondence between simulated molecular dynamics and experimental NMR data (i.e., ^{15}N relaxation and H/D exchange rates) is remarkable. In conclusion, altered local dynamics, entailed by two point mutations, seem to be the underlying reason for the observed increased stability and activity of PG lipase. This study thus illustrates a connection between local dynamics (on the nanosecond timescale), affecting the stability of elements of secondary structure, and thermodynamic stability of the enzyme lipase. This result is thus complementary to previous work showing a correlation between local mobility (likewise probed by NMR relaxation measurements) and enzyme kinetics (Eisenmesser et al. 2002) and offers a rationale for the likewise observed altered lipase activity.

Materials and methods

Sample preparation and enzyme activity measurements

Bacillus subtilis strains containing either the native or PG variant were fermented at a shake flask scale utilizing a defined media, with ^{15}N-labeled urea as the only nitrogen source. 2 L of cultures were harvested by pooling all cultures together, and cells were removed by centrifugation. The supernatants were filtered using a 0.45-μm filter unit, and the cell-free broth was then tested for lipase activity using a synthetic substrate and was concentrated fivefold. The concentrate was applied to an equilibrated (with 25 mM HEPES at pH 8.0 and 1 M ammonium sulfate) POROS-ET (HIC resin) 60-mL column using a mixture of sample with 1 M ammonium sulfate (200 mg of lipase loaded per run). Once the entire sample was loaded onto the column, the column was then washed with 25 mM HEPES (pH 8.0) buffer and 1 M ammonium sulfate (10 column volumes). The lipase was eluted by using a decreasing gradient from the wash condition to 25 mM MES (pH 5.5) buffer. Fractions were collected during the gradient and subsequent MES buffer wash; these fractions were assayed for lipase activity, and only those with the highest activity were pooled together. Pooled fractions were then concentrated with a 10,000 MW cutoff membrane twofold and then dialyzed against 25 mM MES (pH 5.5) to ensure that all of the salt was removed from the sample. The dialyzed sample was removed from the tubing and filtered through a 0.45-μm filter, and then applied to an 80-mL HS (high-density, sulfopropyl cation exchange) column previously equilibrated with 25 mM MES (pH 5.5) buffer. Once the whole sample was loaded onto the column, the column was washed with 10 column volumes of 25 mM HEPES (pH 8.0) to further separate the lipase from any background protein contaminants. Elution of the pure lipase was accomplished with a 15 column volume gradient to 25 mM HEPES (pH 8.0) and 100 mM sodium chloride, with fractions being collected across the gradient. After assaying the fractions for lipase activity, those with the highest activity were pooled together and concentrated using a 400-mL stirred cell and a 5-K membrane. The sample dialyzed overnight against 15 mM sodium acetate (pH 5.5).

Backbone assignment

All NMR experiments were performed at 313 K, typically using 0.6 mM lipase samples in a 20 mM acetate buffer at pH 5.7 with a 1.5 excess of inhibitor *E600*. For the backbone assignment of wild-type and PG mutant lipase, two sets of 2D ^{15}N-HSQC, 2D ^{13}C-HSQC, 3D HNCO, 3D HNCA, 3D HNCACB, and 3D CBCA(CO)NH were recorded on a Bruker DRX600 spectrometer equipped with a cryogenic probe using ^{15}N-^{13}C labeled samples (Sattler et al. 1999). For each ^{15}N-labeled protein, a 3D NOESY-^{15}N-HSQC was recorded on a Bruker DRX750. All spectra were processed with NMRPipe (Delaglio et al. 1995) and visualized using NMRView 5.0.4 (Johnson and Blevins 1994). A modified version of the smartnotebook 3.2 tool integrated in NMRView was used to semi-automatically assign the protein backbones. The smartnotebook module allows visual inspection of the backbone sequential connectivities and provides tools to assign segments of residues to the primary sequence based on characteristic carbon chemical shifts. The connection file listing all possible pairs of residues (i,j) related by their CA(i),CA(j-1),CB(i),CB(j-1) chemical shifts with a given tolerance is determined only once at the beginning of the procedure from backbone triple resonance experiments. The most important feature that we added to the smartnotebook module is the ability to update the connection files at any time upon modification of peak lists during the assignment process. The assigned chemical shifts of both wild-type and PG mutant lipase were deposited in BioMagResonBank under accession numbers 6935 and 6832, respectively.

^{15}N relaxation experiments

All relaxation experiments were performed at 313 K on a Bruker DRX600 spectrometer (^{1}H frequency of 600.28 MHz) using ^{15}N-labeled samples with a concentration of ~0.2 mM and 0.6 mM for wild-type and PG mutant protein, respectively. ^{15}N T_1 and heteronuclear ^{15}N $\{^{1}H\}$-NOE values were determined using the experiments described previously (Farrow et al. 1994). T_1 times were extracted from nine spectra with different values for the relaxation delay: 100 (2×), 200 (2×), 300, 400, 500, 700, 800, 1000, and 1200 msec, applying 180° pulses on protons every 5 msec to suppress chemical shift anisotropy/dipole-dipole CSA(^{15}N)/DD(HN) cross-correlated relaxation. The heteronuclear NOE was recorded seven and two times for the wild-type and PG mutant samples, respectively, with the protons being saturated by 120° pulses (20.7 kHz). ^{15}N T_2 relaxation times were extracted from $T_{1\rho}$ experiments (Peng et al. 1991; Sattler et al. 1999). The $T_{1\rho}$ experiments were recorded with spin-lock pulses of varying lengths 14, 18 (2×), 28, 38, 58 (2×), 78, 108, 158 msec (Houben et al. 2004). Relaxation parameters were extracted with the program Curvefit, using a two-parameter fitting and a Monte Carlo simulation to estimate the errors.

The reduced spectral density approach (Peng and Wagner 1992; Farrow et al. 1995; Ishima et al. 1995) was used to evaluate the relaxation rates (Korzhnev et al. 2002), where the spectral density values around the proton frequency (ω_H and $\omega_H \pm \omega_N$) can be assumed to be all equal to $J(\omega_H)$ and $J(\omega_H+\omega_N)$. Theoretical curves for isotropic rigid body tumbling are represented as black lines in the spectral density plots (Fig. 2).

H/D exchange

Proton-deuterium (H/D) exchange experiments were performed by lyophilizing a ^{15}N-labeled sample and redissolving it in D_2O, thereby monitoring the loss of intensity of labile protons by recording series of ^{15}N-HSQC spectra at 313 K, pD 5.8 and with a concentration of ~0.50 mM for both PG and wild type. The elapsed time between dissolving the lyophilized protein and starting the first ^{15}N-HSQC experiment was 10 min for both proteins. 85 ^{15}N-HSQC spectra were measured between 10 min and 52 d after dissolving the protein. Samples were stored at 313 K between experiments. Measured intensities (I) were fitted to a single exponential decay $I = I_0 \exp(-k_{ex}t) + c$, where I_0 is the amplitude of the exchange curve, k_{ex} is the observed hydrogen exchange rate constant, and the constant c is the peak intensity at the infinity time point. The extracted rates were converted into protection factors (PF) using $PF = k_{int}/k_{ex}$, where k_{int} is the intrinsic exchange rate given at a certain pH (Bai et al. 1993, 1995a; Connelly et al. 1993). Under EX2 conditions, the equilibrium between the "open" state, in which the amide proton is exchange-competent, and the "closed" state, in which the amide proton is protected against exchange, the free energy difference (ΔG) between the closed and the open states is given by:

$$\Delta G = -RT \ln(1/PF)$$

The Gibbs energy calculated from this event would be equal to the global Gibbs energy for global unfolding, as measured by other techniques, if only two states were accessible to a protein, as all amide groups that are protected in the native state would be exposed to the solvent by the same unfolding event. However, for most proteins, the pattern of protection factors shows significant variations between residues (Sadqi et al. 1999 and references therein), indicating that certain amide groups can become exposed to the solvent as a result of local rather than global unfolding events.

Denaturation monitored by far-UV CD, fluorescence, and DSC

All denaturation experiments were performed in Granada. Protein concentrations were measured by UV absorption at 259 nm using a Perkin Elmer Lambda 2S spectrometer. All far-UV CD studies were performed on a Jasco 715 spectrometer using a quartz cuvette with a path length of 1 mm. Temperature-induced unfolding was followed by monitoring the change in ellipticity at 220 nm of 12-μM solutions of protein in 20 mM NaAc (pH 5.8). Samples were heated using a scan rate of 1 K/min. Differential Scanning Calorimetry (DSC) experiments were carried out using a DASM 4 instrument with capillary cells of 0.47 mL, under a constant pressure of 2.5 atm and at a heating rate of 2 K/min of 106-μM solutions of protein in 20 mM NaAc (pH 5.8). Before the cell was filled, the samples were extensively dialyzed against the appropriate buffer solution.

Steady-state fluorescence spectroscopy was carried out with a luminescence spectrometer, LS50B (Perkin-Elmer), using a quartz cuvette with a path length of 1 cm. The excitation wavelength was 280 nm with a band-pass of 7 nm, and the emission spectra were recorded from 300 to 400 nm with a band-pass of 10 nm. The urea transition curve at 25°C was obtained by addition of an appropriate amount of a 10 M urea stock solution resulting in solutions containing the same amount of protein but different final concentrations of urea (12 μM protein in 20 mM NaAc at pH 5.8). The concentrations of urea were checked by refractive index measurements as described by Pace (1986). The urea-induced denaturation was monitored by the change in fluorescence intensity at 323 nm for all proteins. The transition curves were fitted to the two-state model as described previously (Van Nuland et al. 1998).

Molecular dynamic simulations

The molecular dynamics simulations were performed with GROMACS 3.1.4 (Berendsen et al. 1995; Lindahl et al. 2001), using the GROMOS96 43A1 force field (Daura et al. 1998). The simulations were run for 20 nsec at 300 K starting from the lipase wild-type crystal structure fully immersed in explicit water using the SPC model (Berendsen et al. 1981). A second simulation was run for the PG mutant generated from wild-type crystal structure. Analysis of the trajectories was performed using the programs included in the GROMACS package as well as some in-house scripts.

The proteins were solvated in a cubic box of explicit water with a minimum solute-box distance of 14 Å. Five chloride counter-ions were added in each case to electro-neutralize the system. The systems comprised each 20,906 SPC molecules, corresponding to a total number of 65,233 and 65,245 atoms for the wild-type and PG mutant systems, respectively. Periodic boundary conditions were applied. Each system was first energy minimized using 1000 steps of Steepest Descent (SD) algorithm.

The equilibration of each system was performed in five 20-psec phases during which the force constant of the position restraints term for the solute was decreased from 1000 to 0 KJ mol^{-1} nm^{-2} (1000, 1000, 100, 10, and 0 KJ mol^{-1} nm^{-2}, respectively). The initial velocities were generated at the desired temperatures following a Maxwellian distribution. All simulations were performed in the NPT ensemble by weakly coupling the system to external temperature and pressure baths (Berendsen et al. 1984) except for the first 20-psec equilibration part, which was performed at constant volume (NVT).

A 4-fsec time step was used for the leapfrog algorithm integration. The LINCS algorithm (Hess et al. 1997) was used for bond length constraining in conjunction with dummy atoms for the aromatic rings and amino group in side chains (Feenstra et al. 1999), allowing the use of the longer integration time step of 4 fsec. Protein, solvent, and counter-ions were coupled separately to a temperature bath with a time constant of 0.1 psec. The pressure was coupled to an external bath at 1 bar with a time constant of 0.5 psec and a compressibility of 4.5×10^{-5} bar^{-1}. The generalized reaction field (Tironi et al. 1995) was used with a dielectric constant of 54 beyond the 1.4-nm cut-off. The nonbonded pair list was updated every five MD steps.

Data deposition

The ^{1}H, ^{13}C, and ^{15}N backbone assignments of wild-type and PG lipase have been deposited at the BioMagResBank

(http://www.bmrb.wisc.edu) under accession numbers 6935 and 6832, respectively.

Electronic supplemental material

Figure S1 shows the backbone positional RMSD from the starting crystal structure, and electrostatic and van der Waals energies as a function of the MD simulation time. Figure S2 shows the B-factors as a function of the residue sequence as calculated from the last 10 nsec of the MD simulation of the wild-type and the PG mutant lipase. Table S1 reports the calculated spectral density values for wild-type lipase. Table S2 reports the calculated spectral density values for PG lipase. Table S3 reports the slowing factor {log(kc/kex)} calculated form H-D exchange deuterium data for both PG and wild-type proteins.

Acknowledgments

Financial support from the Softlink Program (project no. 01SL057) of the Foundation for Fundamental Research on Matter of the Netherlands (FOM) is gratefully acknowledged. We thank Dr. Tammo Diercks for helpful suggestions and careful reading of this manuscript.

References

Aurora, R. and Rose, G.D. 1998. Helix capping. *Protein Sci.* **7:** 21–38.

Azuaga, A.I., Canet, D., Smeenk, G., Berends, R., Titgemeijer, F., Duurkens, R., Mateo, P.L., Scheek, R.M., Robillard, G.T., Dobson, C.M., et al. 2003. Characterization of single-tryptophan mutants of histidine-containing phosphocarrier protein: Evidence for local rearrangements during folding from high concentrations of denaturant. *Biochemistry* **42:** 4883–4895.

Bai, Y. and Englander, S.W. 1996. Future directions in folding: The multi-state nature of protein structure. *Proteins* **24:** 145–151.

Bai, Y., Milne, J.S., Mayne, L., and Englander, S.W. 1993. Primary structure effects on peptide group hydrogen exchange. *Proteins* **17:** 75–86.

Bai, Y., Englander, J.J., Mayne, L., Milne, J.S., and Englander, S.W. 1995a. Thermodynamic parameters from hydrogen exchange measurements. *Methods Enzymol.* **259:** 344–356.

Bai, Y., Sosnick, T.R., Mayne, L., and Englander, S.W. 1995b. Protein folding intermediates: Native-state hydrogen exchange. *Science* **269:** 192–197.

Berendsen, H.J.C., Postma, J.P.M., van Gunsteren, W.F., and Hermans, J. 1981. Interaction models for water in relation to protein hydration. In *Intermolecular forces* (ed. B. Pullman) pp. 331–342. Reidel Publishing Co., Dordrecht, The Netherlands.

Berendsen, H.J.C., Postma, J.P.M., van Gunsteren, W.F., Di Nola, A., and Haak, J.R. 1984. Molecular dynamics with coupling to an external bath. *J. Chem. Phys.* **81:** 3684–3690.

Berendsen, H.J.C., van der Spoel, D., and van Drunen, R. 1995. GROMACS: A message-passing parallel molecular dynamics implementation. *Comp. Phys. Comm.* **91:** 43–56.

Boston, M., Requadt, C., Danko, S., Jarnagin, A., Ashizawa, E., Wu, S., Poulose, A.J., and Bott, R. 1997. Structure and function engineered *Pseudomonas mendocina* lipase. *Methods Enzymol.* **284:** 298–317.

Chamberlain, A.K., Handel, T.M., and Marqusee, S. 1996. Detection of rare partially folded molecules in equilibrium with the native conformation of RNaseH. *Nat. Struct. Biol.* **3:** 782–787.

Connelly, G.P., Bai, Y., Jeng, M.F., and Englander, S.W. 1993. Isotope effects in peptide group hydrogen exchange. *Proteins* **17:** 87–92.

Daura, X., Mark, A.E., and van Gunsteren, W.F. 1998. Parametrization of aliphatic CH_n united atoms of GROMOS96 force field. *J. Comput. Chem.* **19:** 535–547.

Delaglio, F., Grzesiek, S., Vuister, G.W., Zhu, G., Pfeifer, J., and Bax, A. 1995. NMRPipe: A multidimensional spectral processing system based on UNIX pipes. *J. Biomol. NMR* **6:** 277–293.

Dobson, C.M., Sali, A., and Karplus, M. 1998. Protein folding: A perspective from theory and experiment. *Angew. Chem. Int. Ed.* **37:** 868–893.

Dosset, P., Hus, J.C., Blackledge, M., and Marion, D. 2000. Efficient analysis of macromolecular rotational diffusion from heteronuclear relaxation data. *J. Biomol. NMR* **16:** 23–28.

Eisenmesser, E.Z., Bosco, D.A., Akke, M., and Kern, D. 2002. Enzyme dynamics during catalysis. *Science* **295:** 1520–1523.

Farrow, N.A., Muhandiram, R., Singer, A.U., Pascal, S.M., Kay, C.M., Gish, G., Shoelson, S.E., Pawson, T., Forman-Kay, J.D., and Kay, L.E. 1994. Backbone dynamics of a free and phosphopeptide-complexed Src homology 2 domain studied by ^{15}N NMR relaxation. *Biochemistry* **33:** 5984–6003.

Farrow, N.A., Zhang, O., Szabo, A., Torchia, D.A., and Kay, L.E. 1995. Spectral density function mapping using ^{15}N relaxation data exclusively. *J. Biomol. NMR* **6:** 153–162.

Feenstra, K.A., Hess, B., and Berendsen, H.J.C. 1999. Improving efficiency of large time-scale molecular dynamics simulations of hydrogen-rich systems. *J. Comput. Chem.* **20:** 786–798.

Hess, B., Bekker, H., Berendsen, H.J.C., and Fraaije, J.G.E.M. 1997. LINCS: A linear constraint solver for molecular simulations. *J. Comput. Chem.* **18:** 1463–1472.

Houben, K., Dominguez, C., van Schaik, F.M., Timmers, H.T., Bonvin, A.M., and Boelens, R. 2004. Solution structure of the ubiquitin-conjugating enzyme UbcH5B. *J. Mol. Biol.* **344:** 513–526.

Ishima, R., Yamasaki, K., Saito, M., and Nagayama, K. 1995. Spectral densities of nitrogen nuclei in *Escherichia coli* ribonuclease HI obtained by ^{15}N NMR relaxation and molecular dynamics. *J. Biomol. NMR* **6:** 217–220.

Jaeger, K.E., Dijkstra, B.W., and Reetz, M.T. 1999. Bacterial biocatalysts: Molecular biology, three-dimensional structures, and biotechnological applications of lipases. *Annu. Rev. Microbiol.* **53:** 315–351.

Johnson, B.A. and Blevins, R.A. 1994. NMR view—A computer program for the visualization and analysis of NMR data. *J. Biomol. NMR* **4:** 603–614.

Kay, L.E., Torchia, D.A., and Bax, A. 1989. Backbone dynamics of proteins as studied by ^{15}N inverse detected heteronuclear NMR spectroscopy: Application to staphylococcal nuclease. *Biochemistry* **28:** 8972–8979.

Korzhnev, D.M., Skrynnikov, N.R., Millet, O., Torchia, D.A., and Kay, L.E. 2002. An NMR experiment for the accurate measurement of heteronuclear spin-lock relaxation rates. *J. Am. Chem. Soc.* **124:** 10743–10753.

Korzhnev, D.M., Karlsson, B.G., Orekhov, V.Y., and Billeter, M. 2003. NMR detection of multiple transitions to low-populated states in azurin. *Protein Sci.* **12:** 56–65.

Lindahl, E., Hess, B., and van der Spoel, D. 2001. GROMACS 3.0: A package for molecular simulation and trajectory analysis. *J. Mol. Model. (Online)* **7:** 306–317.

Pace, C.N. 1986. Determination and analysis of urea and guanidine hydrochloride denaturation curves. *Methods Enzymol.* **131:** 266–280.

Peng, J.W. and Wagner, G. 1992. Mapping of the spectral densities of N-H bond motions in eglin c using heteronuclear relaxation experiments. *Biochemistry* **31:** 8571–8586.

Peng, J.W., Thanabal, V., and Wagner, G. 1991. 2D heteronuclear NMR measurements of spin-lattice relaxation-times in the rotating frame of X nuclei in heteronuclear HX spin systems. *J. Magn. Reson.* **97:** 359–395.

Prompers, J.J., Groenewegen, A., Van Schaik, R.C., Pepermans, H.A., and Hilbers, C.W. 1997. ^{1}H, ^{13}C, and ^{15}N resonance assignments of *Fusarium solani pisi* cutinase and preliminary features of the structure in solution. *Protein Sci.* **6:** 2375–2384.

Prompers, J.J., Groenewegen, A., Hilbers, C.W., and Pepermans, H.A. 1999. Backbone dynamics of *Fusarium solani pisi* cutinase probed by nuclear magnetic resonance: The lack of interfacial activation revisited. *Biochemistry* **38:** 5315–5327.

Sadqi, M., Casares, S., Abril, M.A., Lopez-Mayorga, O., Conejero-Lara, F., and Freire, E. 1999. The native state conformational ensemble of the SH3 domain from α-spectrin. *Biochemistry* **38:** 8899–8906.

Sattler, M., Schleucher, J., and Griesinger, C. 1999. Heteronuclear multidimensional NMR experiments for the structure determination of proteins in solution employing pulsed field gradients. *Prog. Nucl. Magn. Reson. Spectrosc.* **34:** 93–158.

Tironi, I.G., Sperb, R., Smith, P.E., and Vangunsteren, W.F. 1995. A generalized reaction field method for molecular-dynamics simulations. *J. Chem. Phys.* **102:** 5451–5459.

Van Nuland, N.A., Meijberg, W., Warner, J., Forge, V., Scheek, R.M., Robillard, G.T., and Dobson, C.M. 1998. Slow cooperative folding of a small globular protein HPr. *Biochemistry* **37:** 622–637.

Wishart, D.S. and Sykes, B.D. 1994. The ^{13}C chemical-shift index: A simple method for the identification of protein secondary structure using ^{13}C chemical-shift data. *J. Biomol. NMR* **4:** 171–180.